QUALITATIVE AND QUANTITATIVE ANALYSES OF ULTRAFINE ANTHRACITE BY FOURIER TRANSFORM INFRARED SPECTROSCOPY AFTER MECHANOCHEMICAL PREPARATION **

Z. Zhu [1], H. Ren [1], L. Wei [1], X. Zhang [1], J. Cao [2], J. Zhu [1*], Y. Liu [1*], H. Bai [3]

[1] School of Materials Science and Engineering at Anhui University of Science and Technology, Huainan, 232001, China; e-mail: longinces@126.com
[2] Huainan Health School in Anhui Province, Huainan, 232007, China
[3] State Key Laboratory of High-Efficiency Utilization of Coal and Green Chemical Engineering at Ningxia University, Yinchuan 750021, China

Comminution is widely used in the deep processing of coal resources. Different chemical structures in coals can influence follow-up procedures significantly. A planetary ball mill was used as a comminution device, and its effects on the grain size and chemical structure of anthracite from Ningxia, China were studied. Comminution kinetics were studied and qualitative and quantitative analyses of functional groups were done by IR spectrometry. The results demonstrate that product size distribution of anthracite from Ningxia conformed to the n-order kinetic model and the grain size reached −42 nm after 24 h. The peak intensity of the IR spectra increased markedly, and the surface activity of anthracite powder was enhanced after ultrafine comminution. Penta-substituted benzene rings of aromatic hydrogen were the dominant group in raw anthracite, while tris-substituted benzene rings of aromatic hydrogen became the dominant form after 24 h of ultrafine comminution. During ultrafine comminution, cyclization of aliphatic chains, dehydroaromatization of cycloparaffin, substitution reactions of orienting groups on aromatic rings, and decarboxylic reactions of benzene rings might occur. Although raw anthracite shows a relatively high degree of metamorphism, its particles show stronger activity and can absorb more oxygen after ultrafine comminution, thus increasing oxygen enrichment. The CH in the aliphatic hydrocarbons of ultrafine anthracite basically disappeared, and CH_2 was more easily lost than CH_3 during ultrafine comminution. Oxygen-containing functional groups in anthracite were altered or some of their elements reacted with oxygen, which decreased the amount of free OH groups on anthracite particle surfaces. During ultrafine comminution, the stability of hydrogen bonds was ranked OH…π > OH…OH > free OH groups > OH…ether > OH…N > cyclic OH tetramers. These changes indicate that the ultrafine anthracite comminution process is also accompanied with chemical reactions. The results provide a reference and guidance for exploring changes in the molecular structures of ultrafine anthracite and follow-up deep processing. In particular, the occurrence of mercaptan -SH and FeS_2 implies that sulfur exists in anthracite in both organic and inorganic forms. The absorption peak of ultrafine pulverized kaolinite was intensified, indicating that minerals were dissociated and more impurities were exposed after comminution.

Keywords: *anthracite, Fourier transform infrared spectroscopy, functional groups, ultrafine comminution.*

**Full text is published in JAS V. 88, No. 6 (http://springer.com/journal/10812) and in electronic version of ZhPS V. 88, No. 6 (http://www.elibrary.ru/title_about.asp?id=7318; sales@elibrary.ru).

КАЧЕСТВЕННЫЙ И КОЛИЧЕСТВЕННЫЙ АНАЛИЗ УЛЬТРАТОНКОГО АНТРАЦИТА МЕТОДОМ ИК-ФУРЬЕ-СПЕКТРОСКОПИИ ПОСЛЕ МЕХАНОХИМИЧЕСКОЙ ПОДГОТОВКИ

Z. Zhu [1], H. Ren [1], L. Wei [1], X. Zhang [1], J. Cao [2], J. Zhu [1*], Y. Liu [1*], H. Bai [3]

УДК 543.42:622.335

[1] Школа материаловедения и инженерии Аньхойского университета науки и техники, Хуайнань, 232001, Китай; e-mail: longinces@126.com
[2] Школа здоровья Хуайнань в провинции Аньхой, Хуайнань, 232007, Китай
[3] Университет Нинся, Иньчуань, 750021, Китай

(Поступила 27 декабря 2020)

Исследовано влияние измельчения на размер зерен и химическую структуру антрацита. С помощью ИК-спектроскопии изучена кинетика измельчения и проведен качественный и количественный анализ функциональных групп. Гранулометрический состав антрацита из провинции Нинся (Китай) соответствует кинетической модели n-го порядка, размер зерна достигает 42 нм через 24 ч. Интенсивность максимума ИК-спектров заметно увеличивается, а поверхностная активность порошка антрацита возрастает после ультратонкого измельчения. Пентазамещенные бензольные кольца ароматического водорода — доминирующие в неочищенном антраците, трис-замещенные бензольные кольца ароматического водорода становятся доминирующей формой после 24 ч сверхтонкого измельчения. Во время ультратонкого измельчения могут происходить циклизация алифатических цепей, дегидроароматизация циклопарафина, реакции замещения ориентирующих групп в ароматических кольцах и декарбоновые реакции бензольных колец. Необработанный антрацит показывает относительно высокую степень метаморфизма, при этом его частицы проявляют высокую активность и могут поглощать больше кислорода после ультратонкого измельчения, увеличивая обогащение кислородом. Группа CH в алифатических углеводородах ультратонкого антрацита в основном исчезает, а при ультратонком измельчении CH_2 теряется легче, чем CH_3. Кислородсодержащие функциональные группы в антраците изменяются или некоторые из их элементов вступают в реакцию с кислородом, что уменьшает количество свободных групп OH на поверхности частиц антрацита. При ультратонком измельчении стабильность водородных связей оценивается как OH… π>OH… OH>свободные группы OH>OH… эфир>OH… N>циклические тетрамеры OH. Изменения указывают на то, что процесс ультратонкого измельчения антрацита также сопровождается химическими реакциями. Результаты служат справочным материалом и руководством для изучения изменений в молекулярной структуре ультратонкого антрацита и последующей глубокой обработки. В частности, наличие меркаптана -SH и FeS_2 означает, что сера существует в антраците как в органических, так и в неорганических формах. Пик поглощения сверхмелкозернистого измельченного каолинита усиливается, указывая на диссоциацию минералов, и после измельчения они подвергаются воздействию большего количества примесей.

Ключевые слова: *антрацит, ИК-Фурье-спектроскопия, функциональные группы, сверхтонкое измельчение.*

Introduction. Ultrafine comminution is an extended type of comminution that can grind materials into nanoscale particles [1]. Common comminution devices include ball mills [1], planetary ball mills [2], stirred mills [3], and airflow mills [4]. The crystal structure, physical properties, and chemical properties of the material may change with changes in grain size. Such changes are attributed to mechanical and chemical effects [5].

Wang et al. [6] investigated the chemical properties of antibiotic biofermentation residue in the comminution process, finding that the CH_2 and CH_3 groups tended to concentrate in the smaller particles. The reason is that the net-like macromolecular aliphatic structures were cracked into numerous short-chain aliphatic carbons. Wang [3] selected crushed coal samples with six different particle diameters (352 to 15.85 μm) to analyze the influences on coal dust wettability. They found that the wettability and amount of hydrophilic oxygen-containing functional groups were negatively correlated with particle size. Li [4] studied Dong Pang 1/3 coking coal under drop weight impact testing. The results showed that the absorption strength of the in-

termolecular hydrogen bonds declined markedly, and free OH groups experienced mechanical-power chemical reactions. Guo [7] ground coal gangue and found that the hydroxyl was removed from the kaolinite, and the structure of the kaolinite deformed after 20 h. Luo et al. [6] investigated the effect of ball mill grinding on the functional groups of bituminous coal and anthracite coal. The results showed that the smaller particles had higher contents of oxygen-containing functional groups and lower concentrations of C–C and C–H than the larger particles had. Zhao [8] investigated the chemical structures of Zhundong coal ground to various particle sizes via a planetary ball mill. According to the results, C–O structures were concentrated in the midsized particles, whereas C=O structures were concentrated in the smallest particles. Subsequently, a comprehensive IR structural parameter showed a good positive correlation with the pyrolysis reactivity.

The alteration of functional groups on the surface of anthracite particles influences the utility of anthracite-based carbon materials. Xiao et al. [9] discussed the influences of oxygen-containing functional groups on the performance of a graphene supercapacitor. They found that oxygen-containing functional groups influenced capacitive performance substantially more than the electrical conductivity and specific surface area did. Xie discovered that nitrogenous basic functional groups on the surface determine the applicability of active carbons to drinking water purification [10]. Abundant hydrogen bonds in coal molecules play an important role in increasing the transformation rate and use of coals [11, 12].

Fourier transform IR (FT-IR) has been widely applied in qualitative and quantitative analyses of the chemical structures of coals [13, 14]. In this study, ultrafine Ningxia anthracite was prepared via a planetary ball mill, and changes in grain size and surface chemical structures before and after comminution were investigated.

Experimental. A planetary ball mill (QM-3SP2, Nanjing Boyuntong Instrument Technology, China) was used as a comminution device. The working principle of the planetary ball mill is shown in Fig. 1. Specifically, the rotating speed was 250 rpm, and the inner diameter of the stainless steel, ball mill tank was 45 mm. Stainless steel balls with sizes of 6.4, 9.5, and 12.7 mm were used. The specific surface area of the media was 77.28 mm^2/g.

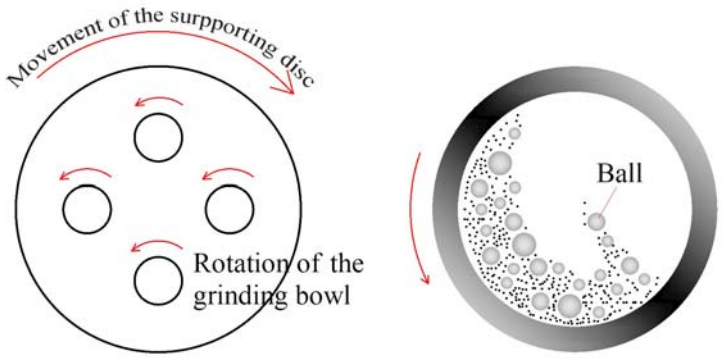

Fig. 1. Working principle of the planetary ball mill.

Anthracite obtained from Ningxia Province China was used as the starting raw material. It was ground and sieved to a uniform size range of 0.2 to 0.3 mm. The proximate and ultimate analyses are shown in Table 1.

TABLE 1. Analysis Results of Raw Anthracite

Proximate analysis (wt%, AD)			Ultimate analysis (wt%, DAF)				
Moisture	Ash	Volatiles	C	H	O	N	S
2.53	7.06	8.96	93.01	3.07	2.49	1.15	0.28

N o t e s: AD = air-dried basis, DAF = dry-ash-free basis. The O content was calculated by difference.

Methods. Raw anthracite (4 g) was mixed with deionized water at a concentration of 14%, and the mixed solution was ground in a planetary ball mill for 24 h. For the first 6 h, samples were collected every 1 h to analyze changes in grain size. After 6 h, to prevent disturbance of the grinding conditions as much as possible, samples were collected every 6 h. The final product obtained after 24 h of comminution was fil-

tered and dried in an electric thermostatic drying oven (DGX-9073B-2, Shanghai Fuma Laboratory Instrument, China). Then the surface functional groups were detected.

Surface chemical analysis was done with an FT-IR spectrometer (Tensor 27, Bruker Optics, Germany). The steps were as follows: 1) Approximately 100 mg of potassium bromide was collected on a piece of weighing paper and put in an agate mortar, in which some anthracite samples (m:KBr = 1:100) were added and mixed completely. The mixture was ground fully. 2) The ground mixture was loaded into a mould, which was then put on a tablet machine and pressurized to 90000 N/cm^2 under vacuum conditions. The pressure was maintained for 1 min. 3) A piece of transparent round sheet that was 0.1 to 1.0 mm thick was selected with tweezers and fixed in a specimen holder. 4) The measurement background was scanned first, and then samples were put in the sample chamber of the IR spectrometer for testing. The samples were scanned 16 times in total.

Grain size was tested by a particle size analyzer (Mastersizer 2000, Malvern Panalytical, UK).

Results and discussion. *Characteristics of ground anthracite*. In the early ultrafine comminution of anthracite, the grain size dropped dramatically. However, the grain size changed only after being subjected to long-term grinding and if enough energy was input as the comminution continued, especially after the grain size reached hundreds of nanometers. The grain size of the samples reached −42 nm after 24 h of comminution in a planetary ball mill (hereafter referred to as ultrafine anthracite). The curve of grain size variation is shown in Fig. 2.

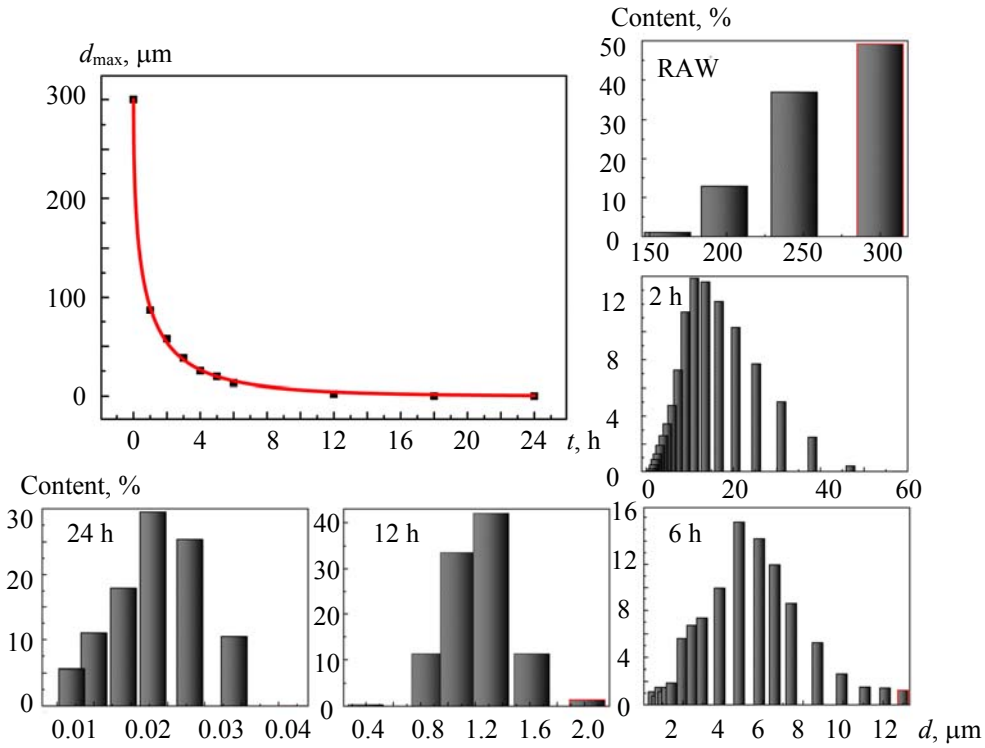

Fig. 2. Variations in grain size during comminution in a planetary ball mill.

Many studies have shown that variations in grain size during comminution conform to an n-order crushing kinetic model [10, 15]. The data points were fitted using the Levenberg–Marquardt algorithm, which provided a good fit ($R^2 = 0.999$). The crushing kinetic equation of anthracite is

$$d_{max} = 300e^{-1.21t^{0.51}}, \quad (1)$$

where e is the natural logarithm, t is time (h), and d_{max} is the maximum grain size in the ground samples (μm).

Infrared spectra before and after comminution. The IR spectra of raw and ultrafine anthracite are shown in Fig. 3. Clearly, the peak intensity of ultrafine anthracite was markedly higher than that of raw anthracite. Ultrafine and raw anthracite showed great differences in the fingerprint region. Fluctuations in the interval of 700–900 reflect great changes in the substitution form of aromatic hydrogen. The sharper peak at 1177 cm^{-1} was attributed to the symmetric elongation of S=O, which shows that there was exposure of sulfides in the anthracite during comminution. Significant differences in the peaks at 1439 cm^{-1} was observed between the

IR spectra of raw and ultrafine anthracite, which were caused by changes in oxygen-containing functional groups. The new characteristic peak at 3034 cm^{-1} was attributed to hydrogen bonds being formed by hydroxyl and N atoms [16, 17].

Figure 3 shows that the absorption peak at 2925 cm^{-1} belonged to asymmetric R_3CH_2. The absorption peak at 2365 cm^{-1} indicated that there might have been –C≡N in the molecular structure of the anthracite. The maximum peak near 1,600 cm^{-1} was caused by the stretching vibration of aromatic ring C=C skeletons, indicating that there were aromatic structures in the molecular structure. Moreover, the aromatic nucleus was the main structure of the aromatic structure. The absorption peaks at 1534 to 1386 cm^{-1} was caused by stretching vibrations (of aromatic ring skeletons) of aromatic C=C, CH_2, and CH_3. The peak at 476 cm^{-1} was caused by –SH, and the absorption peak at 424 cm^{-1} belonged to FeS_2. This indicates that sulfur existed as both organic sulfur and inorganic sulfur.

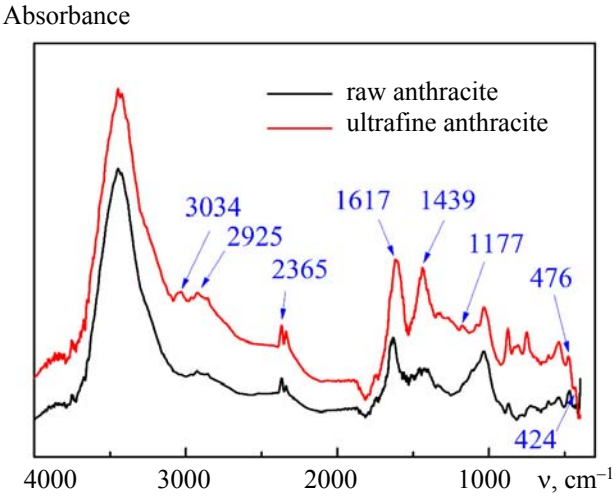

Fig. 3. Infrared spectra of raw anthracite and ultrafine anthracite.

IR spectra of various chemical functional groups. The IR spectrum of anthracite (4000 to 400 cm^{-1}) can generally be divided into four regions [18, 19]; namely, the stretching vibration region of hydroxyl (3000–3600 cm^{-1}), the stretching vibration region of aliphatic series C–H (3000 to 2700 cm^{-1}), the oxygen-containing functional group region (1800 to 900 cm^{-1}), and the out-of-plane deformation vibration region of aromatic C–H (900 to 700 cm^{-1}).

Peak fitting in the main peak region was done using Origin 8.6 (OriginLab Corp., USA) one by one, and the contributions of each peak were determined. All peaks were decomposed into subpeaks in Gaussian function distributions. Hidden peaks were found by the second derivative method, and curves were smoothed by a quadratic polynomial Savitzky–Golay filter.

Figure 4 shows that (a) the peak intensities at 750 and 875 cm^{-1} increased after ultrafine comminution, (b) the absorbance of ultrafine anthracite declined in the interval of 1000 to 1100 cm^{-1}, (c) a new sharp peak occurred at 2880 cm^{-1} after ultrafine comminution, and (d) a sharp peak near 3050 cm^{-1} reflected the formation of new hydrogen bonds or changes in hydrogen bond contents in the ultrafine anthracite.

The principle of IR quantitative analysis is based on the Beer–Lambert law and can be used to investigate and address changes in functional groups [20]. The two main methods are testing the band intensity and measuring the band area [18, 21]. Moreover, calculation methods based on the first and second derivatives of the bands [22, 23] are powerful quantitative analysis methods. In this study, the measurement of band area was applied.

Aromatic hydrogen in anthracite. The results of fitting to the FT-IR spectra of aromatic groups in raw and ultrafine anthracite are shown in Fig. 5. It shows that the aromatic groups changed greatly after ultrafine comminution. A total of 14 peaks were used for fitting to make the fitted spectra closer to the experimental observations. The correlation coefficients were higher than 99.9%.

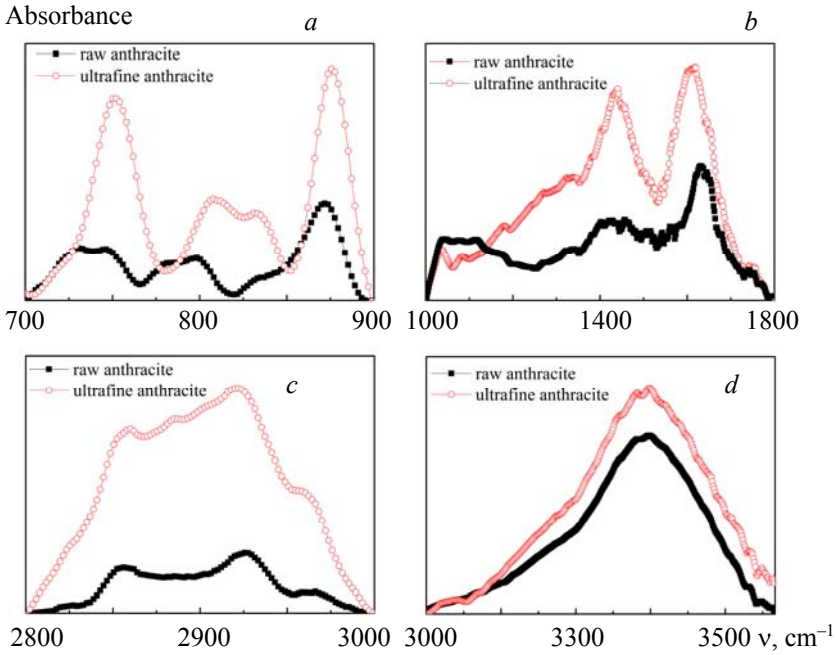

Fig. 4. FT-IR spectra of various regions of raw anthracite and ultrafine anthracite.

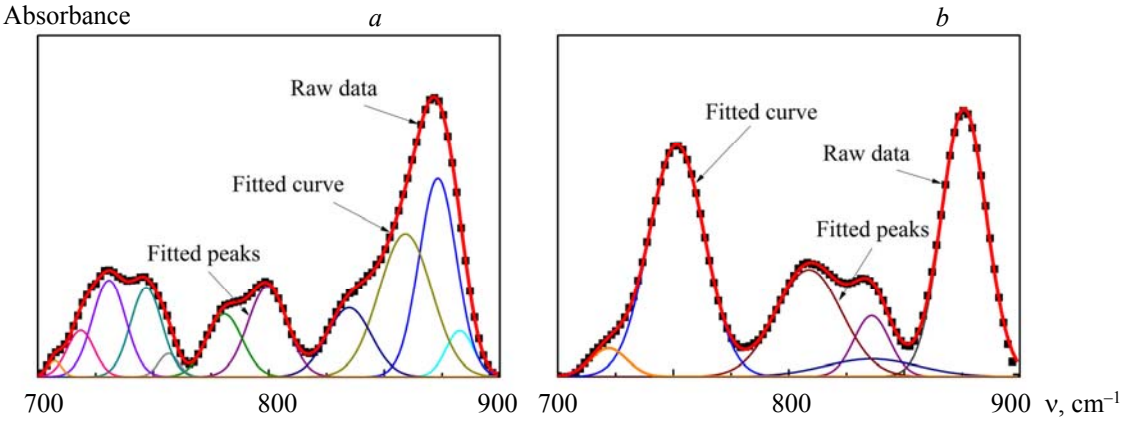

Fig. 5. FT-IR spectra of aromatic hydrocarbons in a) raw and b) ultrafine anthracite.

Anthracite has five aromatic ring substitution forms [18, 24], including a monosubstituted benzene ring at 700 to 710 cm^{-1}, a di-substituted benzene ring at 730 to 750 cm^{-1}, a tris-substituted benzene ring at 750 to 810 cm^{-1}, a tetra-substituted benzene ring at 810 to 850 cm^{-1}, and a penta-substituted benzene ring at 850 to 900 cm^{-1}. The relative contents of different benzene substitution forms in different anthracite samples were obtained according to relevant statistics (Fig. 6). Di-, tris-, tetra-, and penta-substituted benzene rings were the main substitution forms. The penta-substituted benzene ring was dominant (accounting for 40.27%) in raw anthracite, followed by 3-benzene substituted and di-substituted benzene rings, successively. The proportion of monosubstituted benzene rings was only 0.96%. In contrast, tris-substituted benzene rings were the key form in ultrafine anthracite, accounting for 50.83%. Penta-substituted benzene rings accounted for the second-highest proportion (32.92%), while monosubstituted benzene rings disappeared. As the particle size decreased, the long aliphatic side chains or bridge bonds gradually increased [25].

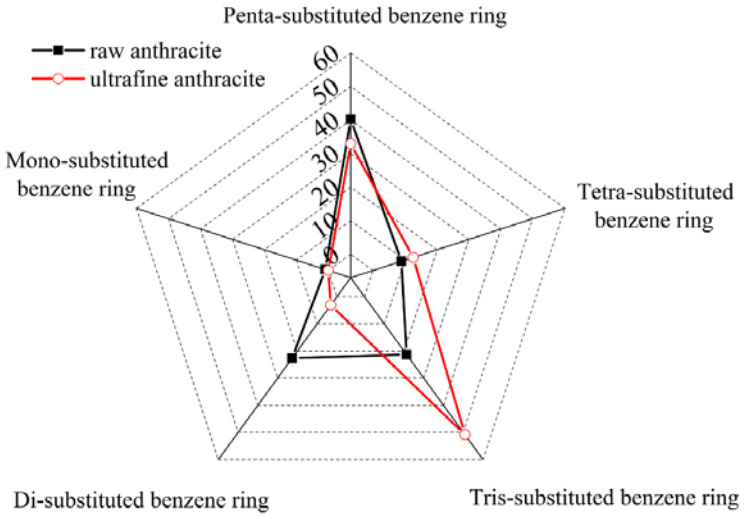

Fig. 6. Contents of various benzene substitution forms in raw and ultrafine anthracite.

Oxygen-containing functional groups in anthracite. The spectral fitting results for the oxygen-containing functional groups of 0.2–0.3 raw and ultrafine anthracite are shown in Fig. 7. The peak at 1450 cm^{-1} was intensified, whereas the peaks in some regions weakened or even disappeared. A total of 18 peaks were selected to make the fitting spectra closer to the experimental spectra, and the correlation coefficients were >99.6%. This waveband contained mainly the stretching vibration of oxygen-containing functional groups. Also, there were vibrations of C=C in the aromatic nucleus and deformation vibrations of methyl and methylene. The main functional groups in anthracite included ether, hydroxyl, carboxyl, carbonyl, and ester groups.

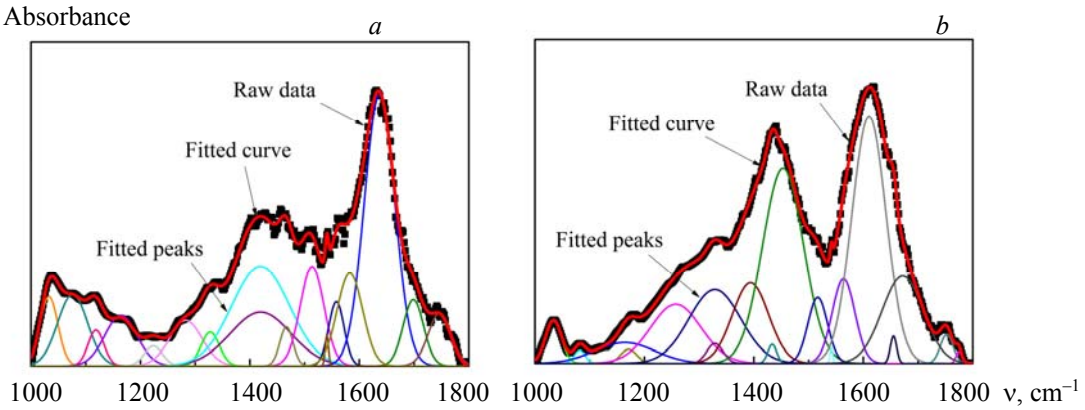

Fig. 7. FT-IR spectra of oxygen-containing functional groups of a) raw anthracite and b) ultrafine anthracite.

The peak of anthracite near 1,030 cm^{-1} was caused by the vibration of Si-O, which is an impure silicate mineral [26]. Due to mutual influences among functional groups, functional groups containing -C–O- presented cross-effects with overlapping peak shapes. The peaks at 1040 to 1260 cm^{-1} were vibration peaks of C–O in alcohol, phenol, ether, phenoxyl, acids, and ester. The peak near 1328 cm^{-1} was caused by the angle-varying vibration of C–H. The peak near 1380 cm^{-1} was attributed to the symmetric angle-variable vibration of methyl. The peaks at 1430 to 1550 cm^{-1} was caused by the vibration of aromatic skeletons. The peak near 1460 cm^{-1} belonged to the asymmetric angle-variable vibration of $-CH_3$ and the deformation vibration of methyl. The peaks at 1610 to 1700 cm^{-1} belonged to the stretching vibration of olefin C=C. The stretching vibration of the C=O of carboxyl was near 1750 cm^{-1}, and the stretching vibration of the C=O of ester was near 1770 cm^{-1}.

The formula (A(C–O) + A(C=O))/A(C=C) was used to determine the degree of oxygen enrichment and was obtained by calculating the areas of the peaks representing C–O, C=O, and C=C in the IR spectrum. In a word, both raw and ultrafine anthracite showed relatively low degrees of oxygen enrichment. This reflects that the raw anthracite had a relatively high degree of metamorphism, resulting in low contents of major elements in the H and O volatile components. However, anthracite particles had stronger activity and could absorb more oxygen after ultrafine comminution, thus enabling greater oxygen absorption. The degree of oxygen enrichment increased from 0.23 to 0.41.

The percentages of C–O, C=C, and C=O in raw and ultrafine anthracite were compared. It was found that the percentage of C–O in ultrafine anthracite was higher than that in raw anthracite, while the percentages of C=C and C=O decreased. As the ultrafine comminution continued, the C=C and C=O in anthracite were destroyed due to continuous energy input. Smaller particles had more active sites and free radicals, which was beneficial to the chemisorption of oxygen [27], whereas C–C and C–H groups were oxidized to C–O groups [28].

Aliphatic hydrocarbon in anthracite. The three types of fatty substances in anthracite are methyl, methylene, and methyne. Both raw and ultrafine anthracite had two absorption peaks near 2860 and 2923 cm^{-1}, which were attributed to the symmetric and antisymmetric stretching vibrations of CH_2 respectively. The peaks at 2960 cm^{-1} corresponded to the symmetric vibration of CH_3, and the peak near 2890 cm^{-1} belonged to the stretching vibration of CH. In this study, six peaks were chosen to make the modelled and experimental spectra closer, and the correlation coefficient was >99.9%. The modelled spectra are shown in Fig. 8.

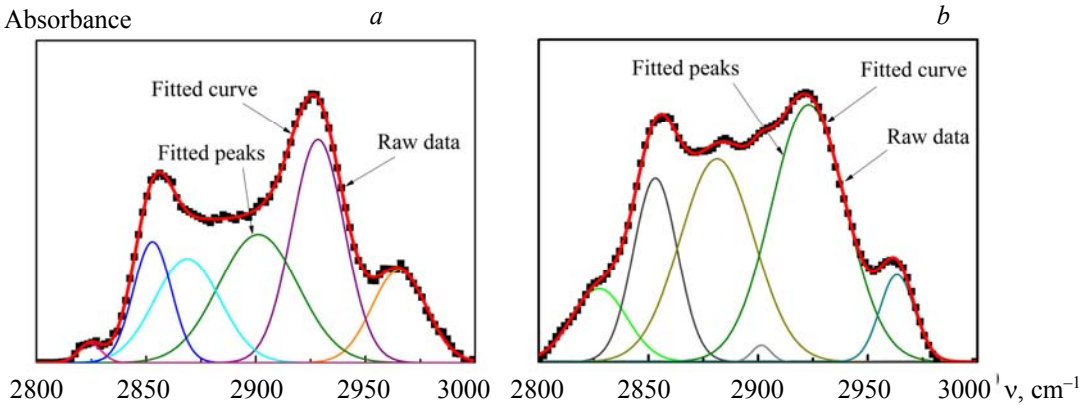

Fig. 8. FT-IR spectra of aliphatic hydrocarbons in a) raw anthracite and b) ultrafine anthracite.

In raw anthracite, the percentages of CH stretching vibrations, CH_2 symmetric and antisymmetric vibrations, and CH_3 symmetric and antisymmetric vibrations were 26.25, 42.12, and 31.63% respectively. These percentages in ultrafine anthracite were 0.63, 54.98, and 44.39%, respectively. To obtain more information about the evolution of aliphatic series, the structural parameter $A(CH_2)/A(CH_3)$ was chosen to evaluate the length and branching degree of the side chains of fatty substances. This parameter was obtained by calculating the area of the peaks representing methyl (CH_3) and methylene (CH_2) in the IR spectrum [29, 30]. The $A(CH_2)/A(CH_3)$ of raw anthracite was 1.33 and that of ultrafine anthracite was 1.24, indicating that CH_2 was more easily lost during ultrafine comminution. This was caused mainly by the continuous breakage of alkyl chains and condensed aromatic rings [27].

Hydrogen bonds in anthracite. According to previous literature, there are seven hydrogen bonds in anthracite [4, 31]. The corresponding absorption peaks are listed in Table 2, and the corresponding molecular structures are shown in Fig. 9 [32].

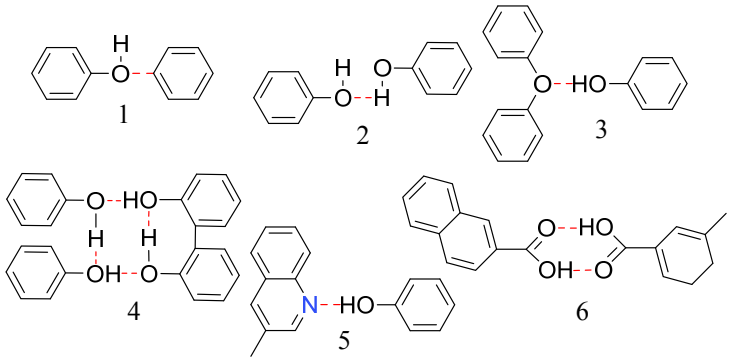

Fig. 9. Molecular structures of various hydrogen bonds in anthracite. 1) OH…π; 2) OH…OH; 3) OH…ether; 4) cyclic OH tetramers; 5) OH…N; 6) COOH…COOH.

TABLE 2. Types of Hydrogen Bonding and Positions of Absorption Peaks in Anthracite

Type of hydrogen bonding	Abbreviation	Position of absorption peak, cm^{-1}
Free OH groups	Free OH groups	3.611
OH and π bonds	OH…π	3.516
Self-association of OH	OH…OH	3.400
OH and O in ether	OH…ether	3.300
Tightly bound cyclic OH tetramers	Cyclic OH tetramers	3.200
OH-N	OH…N	3.100–2.800
COOH dimers	COOH…COOH	2.640

Because the absorption peak at 2640 cm^{-1} was not considered in this study, key attention was paid to changes in the other six hydrogen bonds. To ensure that the spectral models were closer to the observed spectra, six peaks from the experimental spectra were modelled, and the correlation coefficient was >99.9%. It can be seen clearly from the modelled spectra (Fig. 10) that hydrogen bonds formed by self-association of OH made up the highest proportion, reaching 62.43% in raw anthracite and 65.11% in ultrafine anthracite. The relative content of tightly bound cyclic OH tetramers increased from 1.18 to 20.00%. The percentage of hydrogen bonds formed by OH and π bonds was approximately 12%. The content of OH…N increased from 0.14 to 0.70%, which is related to the high content of N in anthracite. The percentage of free OH groups decreased from 6.28 to 0.82% after ultrafine comminution. This may have had two causes: 1) oxygen-containing functional groups in anthracite changed, or some components reacted with oxygen; and 2) the chemical adsorption capacity of -OH weakened due to an uneven charge distribution on the particle surface after ultrafine comminution, thus decreasing the free OH groups on the coal particle surfaces [33].

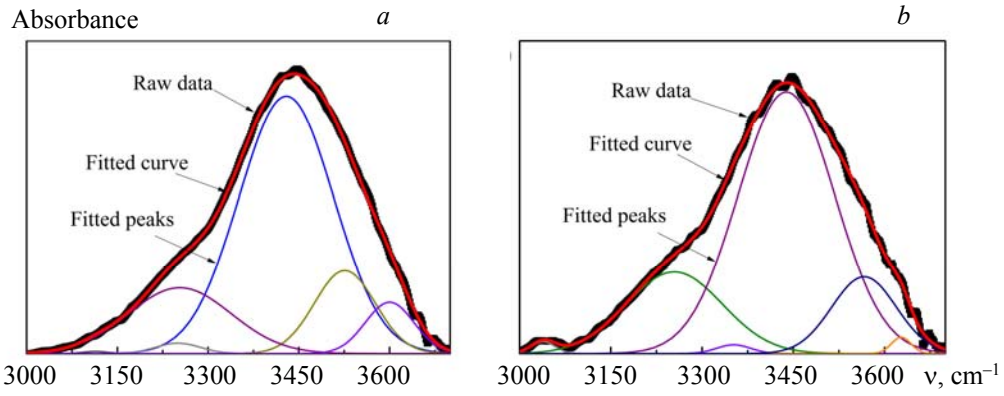

Fig. 10. FT-IR spectra of hydroxyl in a) raw anthracite and b) ultrafine anthracite.

Calculating the absolute variation rate (Table 3) can give the ranking of hydrogen bond stability under fixed comminution conditions: OH…π > OH…OH > free OH groups > OH…ether > OH…N > cyclic OH tetramers.

TABLE 3. Variations in Various Hydrogen Bonds

Classification	Raw anthracite	Ultrafine anthracite	Absolute variation rate (%)
	X	Y	$Z = (Y - X)/X$
OH…N	0.14	0.70	402.64
Cyclic OH tetramers	1.18	20.00	1,594.73
OH…ether	17.14	0.77	−95.52
OH…OH	62.43	65.11	4.30
Free OH groups	6.28	0.82	−86.93
OH…π	12.83	12.60	−1.84

Additionally, the peaks at 3,650 to 3,700 cm^{-1} belonged to kaolinite [34]. More peaks were exposed after ultrafine comminution, accompanied with increases in peak intensity.

Conclusions. Ultrafine anthracite was obtained using a planetary ball mill, and the variation in grain size was analyzed by a laser particle analyzer. Qualitative and quantitative analyses of changes in functional groups were done by FT-IR. The product size distribution of ultrafine Ningxia anthracite conformed to the n-order kinetic model, and the grain size reached −42 nm after 24 h of ultrafine comminution. There were significant changes in various substituted benzene ring contents before and after ultrafine comminution. The monosubstituted benzene rings disappeared. Tris-substituted benzene rings replaced penta-substituted benzene rings as the main component. Anthracite has a high degree of metamorphism and a low degree of oxygen enrichment. After ultrafine comminution, the anthracite particles showed higher activity and could absorb more oxygen. The degree of oxygen enrichment was slightly increased. As the ultrafine comminution continued, C=C and C=O in the anthracite were destroyed with the continuous input of energy. C–C and C–H groups oxidized to C–O groups, causing the percentage of C–O in the ultrafine anthracite to increase. The stretching vibration of CH in ultrafine anthracite decreased substantially, while the percentages of symmetric and antisymmetric vibrations of CH2 and the symmetric and antisymmetric vibrations of CH3 increased. CH2 was more easily lost during ultrafine comminution, which was caused mainly by the continuous breakage of alkyl chains and condensed aromatic rings. The hydrogen bonds formed by the self-association of pH were highest in both raw and ultrafine anthracite. The percentage of free OH groups decreased from 6.28% in the raw anthracite to 0.82% in the ultrafine anthracite. This was because the oxygen-containing functional groups in the anthracite changed, or some components reacted with oxygen. Given a fixed comminution condition, the ranking of the stability of various hydrogen bonds in anthracite was OH…π > OH…OH > free OH groups > OH…ether > OH…N > cyclic OH tetramers.

Acknowledgments. This work was supported by the National Natural Science Foundation of China (Grant No. 51374015), the National Natural Science Foundation of Anhui Province (Grant No. 1708085QE128), and the Foundation of State Key Laboratory of High-efficiency Utilization of Coal and Green Chemical Engineering (Grant No. 2021-K19).

REFERENCES

1. A. Wan, Y. Wu, J. Wang, R. Tu, L. Pan, X. Qi, Y. Liu, *Desal. Water Treat.*, **180**, 126–140 (2020).
2. P. C. Chen, C. Lin, M. H. Chen, P. Y. Chiang, *LWT-Food Sci. Technol.*, **132**, 109848–109856 (2020).
3. P. Wang, X. Tan, L. Zhang, Y. Li, R. Liu, *Proc. Safety Environ. Protec.*, **132**, 189–199 (2019).
4. L. Chengwu, W. Jingui, X. Beijing, D. Lihui, S. Yingfeng, C. Xu, *Spectrosc. Spectr. Anal.*, **34**, 2961–2967 (2014).
5. Q. Zhang, J. Kano, F. Saito, *Handbook of Powder Technology*, **12**, 509–528 (2007).
6. L. Luo, W. Yao, J. Liu, H. Zhang, J. Ma, X. Jiang, *Fuel*, **235**, 1337–1346 (2019).
7. Y. Guo, K. Yan, L. Cui, F. Cheng, *Powder Technol.*, 33–41 (2016).
8. Y. Zhao, P. Qiu, G. Chen, J. Pei, S. Sun, L. Liu, H. Liu, *Fuel*, **189**, 46–56 (2017).
9. X. Peng, W. Dahui, W. Langjun, *J. Electrochem.*, **20**, 553–562 (2014).

10. X. Bu, G. Ma, Y. Peng, G. Xie, H. Zhan, B. Liu, *Int. J. Coal Prep. Util.*., **1**, 1–20 (2019).
11. R. Hou, Z. Bai, H. Zheng, Z. Feng, D. Ye, Z. Guo, L. Kong, J. Bai, W. Li, *Fuel*, **265**, 117011–117020 (2020).
12. L. Dongtao, L. Wen, L. Baoqing, *Chem. Bull.*, **7**, 411–415 (2001).
13. M. L. A. Gil, M. Luna, R. Zarzuela, M. V. García-Moreno, *Vibr. Spectrosc.*, **110**, 103109 (2020).
14. T. Xiao, H. Yuan, Q. Ma, X. Guo, Y. Wu, *Int. J. Biol. Macromol.*, **132**, 1106–1111 (2019).
15. X. Bu, Y. Chen, G. Ma, Y. Sun, C. Ni, G. Xie, *Powder Technol.*, **359**, 305–313 (2020).
16. D. Behera, B. K. Nandi, S. Bhattacharya, *Int. J. Coal Prep. Util.*, **5**, 1–17 (2020).
17. W. Shifu, X. Yizhuang, *Fourier Transform Infrared Spectroscopy*, Chemical Industry Press, Beijing (2016).
18. Y. Zhao, C. Xing, C. Shao, G. Chen, S. Sun, G. Chen, L. Zhang, J. Pei, P. Qiu, S. Guo, *Fuel*, **278**, 118229 (2020).
19. H. Panyun, M. Yanjun, Z. Fangui, Y. Taotao, X. Guangbo, *Spectrosc. Spectral Anal.*, **40**, 787–792 (2020).
20. X. Zhang, S. Zhang, P. Li, Z. Ding, Z. Hao, *Fuel Proc. Technol.*, **174**, 123–131 (2018).
21. X. Cui, X. Li, Y. Li, S. Li, *J. Thermal Anal. Calorimetry*, **129**, 1169–1180 (2017).
22. A. S. Dhaulaniya, B. Balan, K. K. Sodhi, S. Kelly, A. Cannavan, D. K. Singh, *LWT-Food Sci. Technol.*, **131**, 109749–109758 (2020).
23. K. T. Mader, M. Peeters, S. E. L. Detiger, M. N. Helder, T. H. Smit, C. L. Le Maitre, C. Sammon, *Faraday Discuss.*, **187**, 393–414 (2016).
24. L. Huzhen, W. Chuange, Z. Fangui, L. Meifen, X. Jianhua, *J. Fuel Chem. Technol.*, **42**, 129–137 (2014).
25. X. Chen, Y. Zhao, L. Liu, L. Zhang, Z. Zhang, P. Qiu, *J. Anal. Appl. Pyrol.*, **130**, 294–304 (2018).
26. H. Dubin, C. Xiuyun, C. Xi, *Spectrosc. Spectral Anal.*, **3**, 3698–3703 (2016).
27. J. Liu, X. Jiang, J. Shen, H. Zhang, *Adv. Powder Technol.*, **25**, 916–925 (2014).
28. W. Xia, J. Yang, C. Liang, *Appl. Surf. Sci.*, **293**, 293–298 (2014).
29. H. Xiaohong, L. Zhaohui, Y. Zhiqiang, Y. Ming, Z. Tai, *J. Eng. Thermaphys.*, **34**, 969–972 (2013).
30. P. C. Painter, R. W. Snyder, M. Starsinic, M. M. Coleman, D. W. Kuehn, A. Davis, *Appl. Spectrosc.*, **35**, 475–485 (1981).
31. L. Zhanku, W. Haitao, Y. Honglei, Y. Jingchong, L. Zhiping, R. Shibiao, W. Zhicai, *J. Fuel Chem. Technol.*, **48**, 1–7 (2020).
32. K. Mae, K. Miura, *Fuel Energy Abstr.*, **43**, 278 (2002).
33. L. Min, *Research on Oxygen-Containing Functional Groups on Coal Surface*, Thesis, Taiyuan University of Technology (2004).
34. H. Machnikowska, A. Krztoń, J. Machnikowski, *Fuel*, **81**, 245–252 (2002).